Batteries & Supercaps

Research Article
doi.org/10.1002/batt.202200060

Chemistry
Europe
European Chemical
Societies Publishing

www.batteries-supercaps.org

Scaling Methodology to Describe the Capacity Dependent Responses During Thermal Runaway of Lithium-Ion Batteries

Stefan Doose,*[a, b] Alexander Hahn,[a, b] Michael Bredekamp,[a, b] Wolfgang Haselrieder,[a, b] and Arno Kwade[a, b]

In this work, internal short-circuit tests on prototypically battery cells of different cell capacities were performed to determine scalable dependencies of the thermal runaway. It shows that this pouch cells with NMC111/graphite electrodes must have a minimum capacity of 1.5 Ah to develop a thermal runaway. In addition, it could be determined that with increasing battery capacity the strength of the reaction also increases, which is visible, among other things, in the linear temperature increase on the cell surface from 1.5 Ah to 3.0 Ah of overall 66.77 °C and the increasing weight loss, of up to 37.5 % compared to the starting weight. It could also be shown that the processes of the thermal runaway can be described within certain limits by simple linear (cell surface temperatures, penetration depth, time until cell voltage reaches 0 V) and nonlinear fits (cell weight loss, setoff voltage at TR). This allows the determination of scalable parameters and test results with a minimum of test effort. Furthermore, increasing concentrations of the determined substances could be measured for the infrared-active gaseous reaction products. In particular, the decomposition products CO and CO_2, as well as the linear hydrocarbons, increase significantly with increasing capacity. On the whole, parameters for the description of the thermal runaway could be determined, which describe the effects and reactions of the thermal runaway well and could minimize test efforts with known materials.

Introduction

Electrochemical energy storage devices as lithium-ion batteries (LIB) increasingly play an indispensable part in today's society.[1,2] Both the mobility shift towards green technologies and the use of home storage and portable end-user devices are necessitating a number of LIB on the market. LIBs are increasingly in use due to their high power and energy density as well as their good lifetime.[2–4] However, high performance data, especially high energy densities, also harbor risks that should not be underestimated. If LIBs are damaged or used improperly, strong exothermic reactions can occur between the components of the LIB, the so-called thermal runaway (TR).[5,6] During TR, in addition to strong electric currents (e.g., during short-circuiting) under certain circumstances, temperatures of greater than 600 °C occur at the cell surfaces, which initial according to the current heat law are produced by Joule's heat

when current flows through a conductor. The subsequently initiated chemical reactions are mostly exothermic in nature and release large amounts of energy in the form of heat. In addition to energy, many reaction products are released as gaseous components. In particular, hydrogen (H_2), carbon dioxide (CO_2), carbon monoxide (CO) and short-chain hydrocarbons are produced from the electrolyte components used, and fluoride-containing gases such as hydrogen fluoride (HF) are formed from the conducting salt and binder.[7–9]

In order to study the processes taking place at the laboratory level, various methods can be used to initiate the TR, which are divided into mechanical (internal and external short circuit), thermal (furnace or ARC test) and electrical (overcharge, over discharge).[10] A commonly used test, since reliable in initiating TR, is the nail penetration test. In this test, a nail made of conductive or non-conductive material is driven through the layers of the battery cell under test, causing an internal short circuit.[6,11,12] Due to the uncontrolled flow of electrical energy, Joule heat is generated according to the current heat law, which provides the activation energies for the start reactions of the TR.[6,13] First, the solid electrolyte interface (SEI) is decomposed exothermically at temperatures between 90 and 120 °C. Subsequently, the incorporated liquid electrolyte reacts under decomposition with the conducting salt, the anode components and the intercalated lithium. Finally, the cathode active material is decomposed at > 250 °C with strong energy release.[3,7–9] Furthermore, if a critical amount of energy can be generated by the reactions, it can lead to thermal propagation of the TR within modules or even whole battery packs. Since the strength of the reactions depends primarily on the amount

[a] S. Doose, A. Hahn, M. Bredekamp, W. Haselrieder, A. Kwade
Institute for Particle Technology
Technische Universität Braunschweig
38104 Braunschweig, Lower Saxony, Germany
E-mail: s.doose@tu-braunschweig.de

[b] S. Doose, A. Hahn, M. Bredekamp, W. Haselrieder, A. Kwade
Battery LabFactory Braunschweig
Technische Universität Braunschweig
38106 Braunschweig, Lower Saxony, Germany

Batteries & Supercaps

Research Article
doi.org/10.1002/batt.202200060

Chemistry Europe
European Chemical
Societies Publishing

of reactants available for the reactions and also on the amount of energy stored electrochemically, the aim is to carry out tests with the lowest possible hazard potential but with well-founded significance.

In addition to the existing hazard potential, safety tests also involve a not inconsiderable amount of technical equipment and cost. With regard to this point, especially in the case of high capacity cells, the prediction of results, which describe the temperature on the cell surface, the cell stresses and the resulting gas concentrations, is important. In addition, results such as mass loss during thermal runaway, certain stress-based parameters or penetration depths of the nail until the start of thermal runaway can be identified as characteristic and scalable parameters. With the help of these parameters, simple fits (linear and nonlinear) can be used to describe or predict characteristic safety related parameters.

The overall goal of this research is the identification of certain representable characteristic parameters and measurement parameters, whereby nail penetration experiments on cells of different capacities will generate data and enable the prediction of direct measurement data as well as other parameters. The results can help to greatly increase the effort, cost as well as the significance of results with few experiments. So far, the authors are not in the knowledge of any literature addressing scaling and the identification of scalable parameters to describe the TR. For this reason, the presented results are a novelty in this field and allow, within certain limits, the prediction of the TR with very little experimental effort.

Results and Discussion

Within this research paper, nail penetration test with a reliable test methodology[11,12] on custom-made battery cells with different capacity show an influence of the capacity on parameters such as the short-circuit voltage, the resulting temperatures and also gaseous reaction products. In addition, other parameters like the necessary penetration depth, the mass loss due to the thermal runaway and voltage-dependent values can be determined as a function of the capacity. As a goal of the work an approach for the scalable description of the TR of batteries is discussed.

Influence of capacity on electrical and thermal behavior

Figure 1 shows the voltage curves of the battery cells with varied capacity from 1.5 to 3.0 A h after nail penetration over the test time (the test time with reference to the start of the critical voltage drop for better comparability is named relative test time). The data for cells with a 1.0 A h capacity are not presented further below, since no TR could be triggered in these by nail penetration. A typical course of the voltage drop can be seen. After nail penetration, at first the voltage drops slowly to a value between 3.6 and 3.9 V, depending on the penetration depth of the nail. From this value on, the voltage drops fast to 0 V between 3.2 s for 1.5 A h and 5.2 s for 3.0 A h. Here, the voltage is reduced to 0 V. When the voltage drops so fast, there is sufficient energy in the form of Joule heat due to the internal short circuit, so that a thermal runaway occurs. With increasing capacity, as shown by Figure 1 the time for the acute reactions of the thermal runaway increases. The time required from the start of the reactions until 0 V is reached
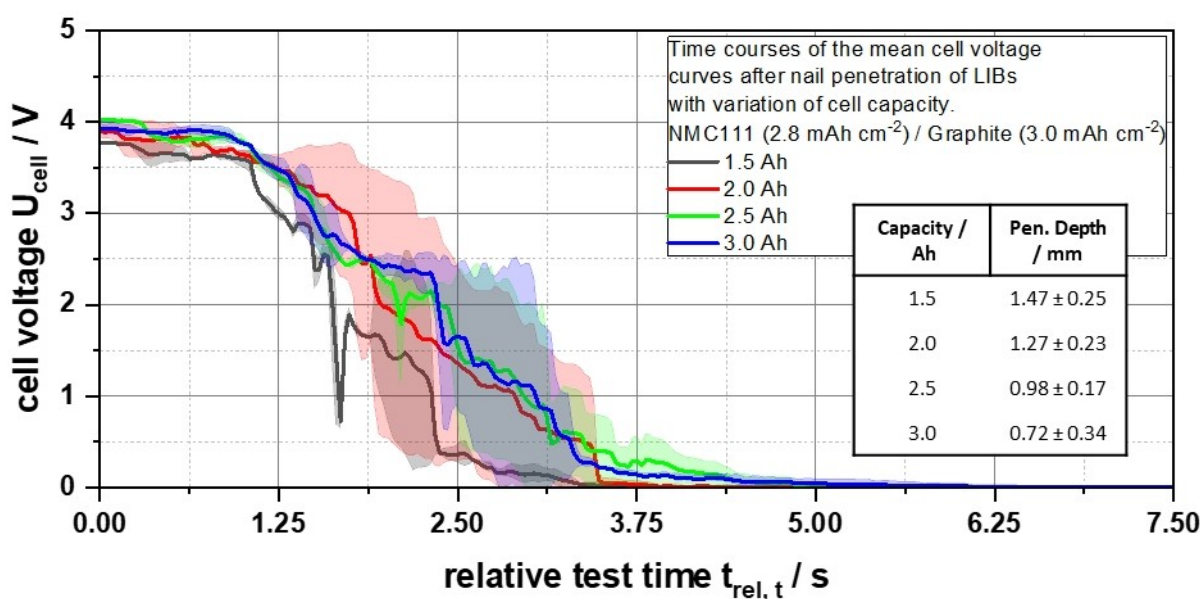

Capacity / Ah	Pen. Depth / mm
1.5	1.47 ± 0.25
2.0	1.27 ± 0.23
2.5	0.98 ± 0.17
3.0	0.72 ± 0.34

Figure 1. Time course of the voltage drop after nail penetration of battery cells with variation of capacity of 1.5 A h (black), 2.0 A h (red), 2.5 A h (green) and 3.0 A h (blue) as well as the resulting penetration depths to the TR with variation of the cell capacity.

Batteries & Supercaps

Research Article
doi.org/10.1002/batt.202200060

Chemistry Europe
European Chemical
Societies Publishing

increases (the exact data for the time to reach 0 V can be taken from Figure 4). In addition, the remaining cell voltage at the start of the rapid voltage drop also increases in relation to the battery capacity. Moreover, the determined penetration depth to the start of the TR decreases from 1.47 ± 0.25 mm (1.5 Ah) to 0.72 ± 0.34 mm with increasing battery capacity. From this it can be deduced that there are still more intact compartments that can supply the damage site with a larger equalizing current and thus, generate more Joule heat with less damage. Based on these results, it can be assumed that with increasing battery capacity at the start of the reaction more available residual energy in the battery cell can be suddenly released. Since in the case of a short circuit, as shown, a high current flow in a short time through a comparatively small conductor, the short circuit point, Joule heat is generated according to the current heat law, depending on the material. The Joule heat provides the activation energy for the chemical chain reactions of the thermal runaway, most of which have exothermic properties. For the 2 Ah battery cells Figure 2 shows the time dependence of the surface temperatures 1, 2 and 3 cm away from the penetration point. With the start of the reactions, a very fast increase of all measured surface temperatures can be observed. Between 11.4 s (1 cm distance) and 14.4 s (2 and 3 cm distance), the temperature values reach their maxima of $580.58\,°C \pm 33.72\,°C$ (1 cm distance), $463.58\,°C \pm 30.03\,°C$ (2 cm distance), and $424.14\,°C \pm 19.42\,°C$ (3 cm distance). Thus, depending on the distance of the penetration point (initial short circuit point), the maximum surface temperatures reached increase with decreasing distance. As the cell surface cools down, the temperatures converge to a common value after approximately 150 s. This can be explained by the fact that during the reaction the thermal runaway reactions first take place at a short distance from the short circuit point and

reactants (especially organic electrolyte components) are consumed to a large extent. Gases and particles are initially discharged from the cell through the penetration point before further openings are formed in the sealing seams (see Figure 3C). In the following the reactions continue in a circular fashion in the cell until the reaction has reached the entire cell. The amount of reactants available continues to decrease, especially the organic electrolyte components, so the further away the reaction center, the lower the temperature.

The influence of the battery capacity on the maximum surface temperatures reached is depicted in Figure 3(A). The tendency of decreasing maximum temperature with increasing distance from the penetration point can be seen for all capacities investigated. In addition, the surface temperatures at the same distance of the penetration point can be reasonably represented with a linear function of the cell capacity, with R^2-values of 0.985 (1 cm distance), 0.889 (2 cm distance), and 0.990 (3 cm distance):

$$T_{S,Max} = a \cdot (\text{cell capacity}) + b$$

The correlating values for the parameters a and b for the mathematical description of the maximum surface temperature at 1, 2, and 3 cm distance from the penetration point are demonstrated in Table 1.

From 1.5 Ah to 3.0 Ah battery capacity the maximum surface temperatures increase at a distance of 1 cm from the penetration point from $557.59\,°C \pm 15.64\,°C$ (1.5 Ah) to $580.58\,°C \pm 33.72\,°C$ (2.0 Ah) to $608.32\,°C \pm 18.64\,°C$ (2.5 Ah) and finally to $624.36\,°C \pm 23.30\,°C$ (3.0 Ah), for example (See Figures S1–S3). With increasing battery capacity, more energy is initially stored in the cell, which means that, as described above, reactions of the TR start earlier (with lower penetration
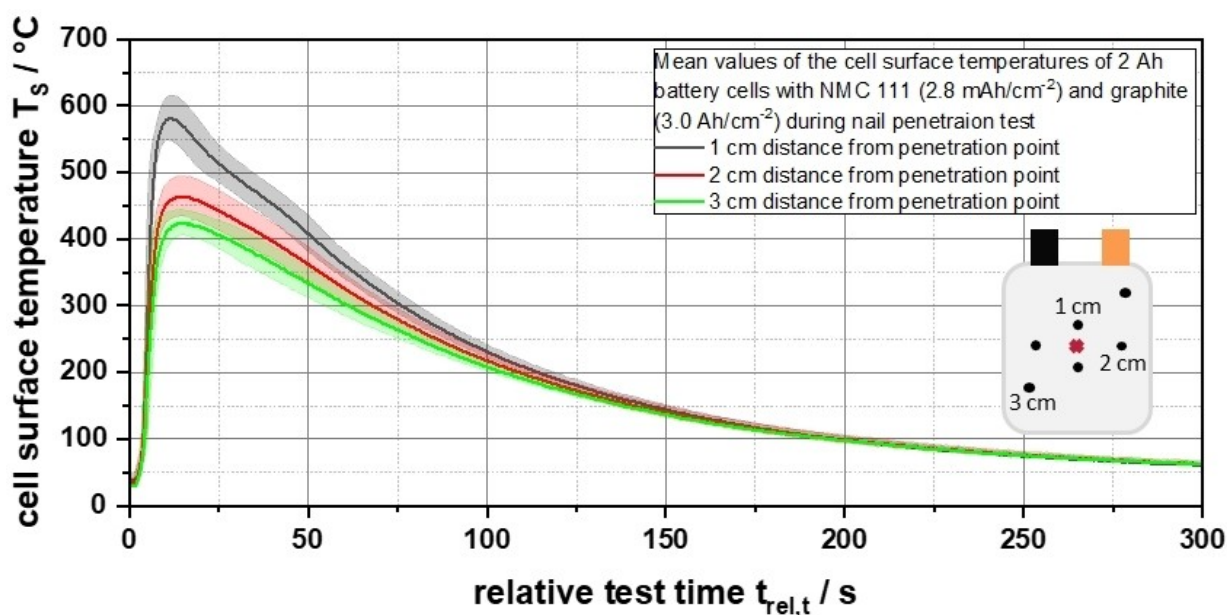

Figure 2. Time course of the mean values of the cell surface temperatures of 2 Ah battery cells in 1 cm (black), 2 cm (red) and 3 cm (green) distance from the penetration point.
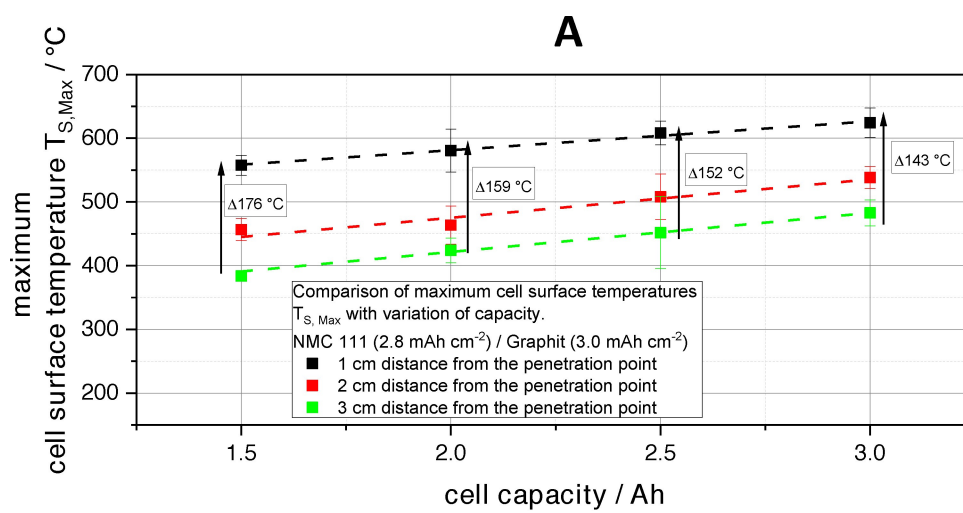
Figure 3. A) Plot of the determined maximum cell surface temperatures at 1 cm (black), 2 cm (red) and 3 cm (green) distance from the defined penetration point as a function of the battery cell capacity; B) X-ray image of a 2 Ah battery cell before nail penetration; C) X-ray image of a 2 Ah battery cell after nail penetration and thermal runaway.

Table 1. Linear fit parameters describing the maximum surface temperature as a function of the cell capacity.

	1 cm distance	2 cm distance	3 cm distance
a [$°C\,A\,h^{-1}$]	45.29 ± 3.17	60.27 ± 12.01	61.37 ± 3.49
b [$°C$]	490.57 ± 7.41	354.64 ± 27.79	298.79 ± 8.72

depth and higher remaining cell voltage) and higher temperatures can be reached. The increasing energy content with increasing battery capacity resulting in higher maximum temperatures can be seen in Figure 3(A). The shown linear fits of the temperatures at the defined distances slightly converge with increasing battery capacity, so that the resulting temperature gradient across the measurement points becomes smaller. 1.5 Ah capacity shows a temperature decrease of 176 °C from 1 cm to 3 cm distance from the penetration point, whereas 3 Ah capacity shows a decrease of 143 °C. Thus, the slope of the fits increases with higher distance to the penetration point. At 1 cm distance a slope of $45.29\,°C\,A^{-1}\,h^{-1}$, at 2 cm distance $60.27\,°C\,A^{-1}\,h^{-1}$ and at 3 cm distance $61.37\,°C\,A^{-1}\,h^{-1}$ can be observed. The decreasing temperature

differences at higher cell capacity led to the conclusion that at increasingly higher capacities, the temperature rise across the cell surface becomes more constant. However, it can be assumed that the temperature outside the investigated range also tends towards a limit value. However, these fits can be used to predict temperature emergence in cells with the chemistry in question and to represent it via linear dependencies.

In summary, the described results show that with increasing battery capacity reactions of the TR start earlier and leave a higher residual energy in the cell at the start of the TR. In addition, a higher energy content of the battery cells leads to increasing surface temperatures, with the possibility of representing these by linear dependencies for the cell chemistry and format used.

Identification of scalable parameters for description of the TR

The approach of scalability of characteristic parameters facilitates the description of the processes during thermal runaway
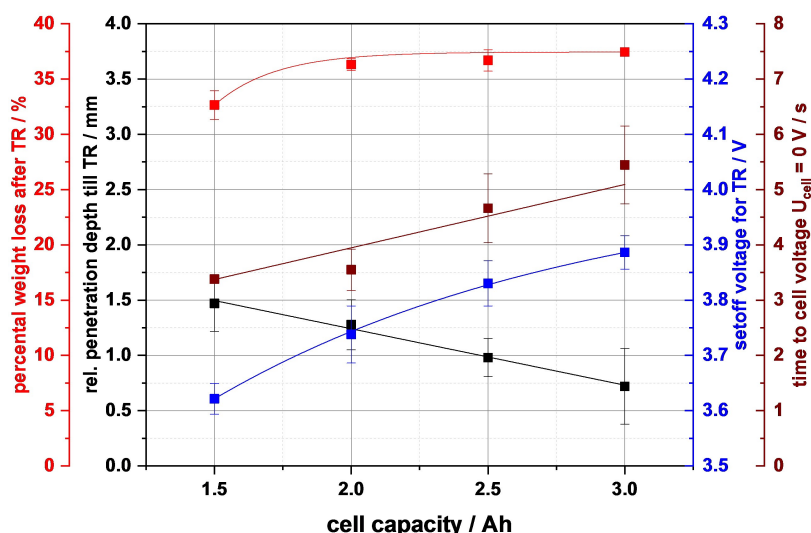
Figure 4. Presentation of identified characteristic parameters and associated fit lines to describe TR depending values above related cell capacity from 1.5 to 3.0 Ah.

and can also be helpful to require smaller test scenarios/series. In the following, characteristic parameters that can be mapped via simple fits are shown Figure 4 and discussed. Some of the parameters have already been shown in the previous chapter to explain the results.

As described in the previous chapter, the extent of the reactions of the TR increases with increasing battery capacity in different ways: On the one hand, more energy is stored in the cell at the start of the TR, higher reactant quantities are available for chemical reactions and higher temperatures are also reached on the surface. In addition to the linear description of the maximum temperatures on the cell surfaces, other parameters can also be described with fits: The penetration depth to TR as well as the time to reach the cell voltage of 0 V can be approximated linearly according to the following equations with the parameters from Table 2:

$$\text{rel. penetration depth} = c \cdot (\text{cell capacity}) + d$$

and

$$U_{cell=0\ V} = e \cdot (\text{cell capacity}) + f$$

The percental weight loss after TR as well as the setoff cell voltage at the start of the TR, on the other hand, can be approximated with the following nonlinear function with the parameters from Table 3:

Table 2. Linear fit parameters describing the relative penetration depth until TR and the time to reach a cell voltage of 0 V as a function of the cell capacity.

	rel. penetration depth	$U_{cell} = 0\ V$
slope	$c = -0.511 \pm 0.034$	$e = 1.147 \pm 0.290$
constant	$d = 2.262 \pm 0.077$	$f = 1.654 \pm 0.448$

Table 3. Non-linear fit parameters describing the percental weight loss and the setoff voltage at the start of the TR as a function of the cell capacity:

	Percental weight loss after TR	Setoff voltage for TR
Y_0	-4197.55	2.83
A_1	2117.5	0.596
t_1	0.22	1.365
A_2	2117.5	0.596
t_2	0.22	1.365

$$y = y_0 + A_1 \cdot \left(1 - e^{\frac{-\text{cell capacity}}{t_1}}\right) + A_2 \cdot \left(1 - e^{\frac{-\text{cell capacity}}{t_1}}\right)$$

With increasing battery capacity, the necessary penetration depth to start the TR decreases linearly from 1.47 ± 0.25 mm to 0.72 ± 0.34 mm. The linear decrease can be explained by the linear increase in battery capacity, since the amount of energy stored in the battery cell increases linearly with the number of electrodes installed in the stack. The start of the uncontrollable reactions of the TR represents the magnitude of the setoff voltage for TR, which shows a non-linear progression inversely proportional to the penetration depth. The remaining voltage increases with the battery capacity and will strive for a limit value below 4.2 V. The two values are directly related because as the damage increases, more energy is released in the form of Joules heat due to the short circuit current. Thus, the TR will start at lower damage with increasing battery capacity. The time required until the cells reach a voltage of 0 V, which means that no more energy can be released from the electro-chemically stored energy, increases linearly with increasing capacity due to the lower damage and the higher setoff voltage still present. In addition, the determined percental weight loss compared to the starting weight of the tested cell shows the effort to reach a limit value of 37.5%. With increasing capacity, the reaction in the cell becomes stronger, as already described. Due to the higher temperatures, a larger

Batteries & Supercaps

Research Article
doi.org/10.1002/batt.202200060

Chemistry Europe
European Chemical
Societies Publishing

amount of gas is produced by chemical reactions, which also increases the discharge of particles from the cell. In addition, it can be assumed that at higher temperatures smaller residual quantities of organic solvents remain in the destroyed cell. The weight loss visualized by X-ray and the resulting transport paths in the cell are shown in Figure 3(B and C) as an example for the 2 Ah cell before (Figure 3B) and after (Figure 3C) penetration. After penetration, the lighter areas in Figure 3, C show the material flow paths out of the cell. The cell bursts preferentially at the sealing seams and the penetration point, discharging particles and hot gases.

In summary, it has been found that selected parameters describing TR can be represented by simple linear and non-linear dependencies in a good way in the tested range of 1–3 Ah battery capacity. This ability to scale allows reactions at known formats and chemistries to be predicted to some extent and to predict outcomes and potential hazards.

Capacity dependent evolution of infrared active gas species

During thermal runaway, triggered by the nail penetration, chemical chain reactions between the components of the LIB are caused by the Joule heat generated during short-circuiting, whereby the reactions are mostly exothermic and thus, self-initiating or self-reinforcing. Essentially, many of the reaction products, in addition to solids, show up as gaseous substances. Figure 5 plots the concentrations over time of CO_2 and CO, two of the main decomposition and reaction products of the electrolyte and anode, against the test time. Regardless of the battery capacity or reaction product tested, a general trend of concentration variation can be observed. After the start of the reaction, a strong initial increase of the concentration occurs until the maximum is reached. After passing through the maximum, a decrease in concentration can be determined over

a period of up to 600 s after reaction. The continuous flushing of the experimental chamber causes the concentration to decline over a long period of time, with the carrier gas N_2 transporting the reaction products into the FTIR used. The cell reaction itself is finished after a short time, when the maximum concentration is reached.

For both reaction products depicted as a function of time, an increase in the maximum concentration achieved can be observed, especially when the battery capacity is increased. The maximum concentration of CO_2 increases from $35,407 \, mg \, cm^{-3} \pm 2,827 \, mg \, cm^{-3}$ (1.5 Ah) to $45,903 \, mg \, cm^{-3} \pm 1,637 \, mg \, cm^{-3}$ (2.0 Ah) and $62,167 \, mg \, cm^{-3} \pm 5,659 \, mg \, cm^{-3}$ (2.5 Ah) to $68,467 \, mg \, cm^{-3} \pm 2,387 \, mg \, cm^{-3}$ (3.0 Ah), although no significant change in the time to reach the maximum was determined. Furthermore, CO is also following this trend. Since the weight of the cell stack also increases linearly with the linearly increasing capacity of the battery cells and the quantity of electrolyte used depends on this, the quantity of gas produced and determined also increases in a similar manner. From 1.5 Ah to 3.0 Ah cell capacity, the determined CO_2 concentration increases by about 2 times. In the case of CO, this increase is even more significant, by a factor of approximately 3. The stronger increase in CO is probably due to the fact that, as a result of the higher temperatures reached (cf. Figures 2 and 3), a larger proportion of the electrolyte components have reacted to form CO. At lower capacities, it can be assumed that a larger percentage by mass of these are still present in their original form. In addition, the reactions were carried out under an inert gas atmosphere, as a result of which the formation of CO occurs preferentially, since the availability of oxygen is limited. In Figure 6, the maximum concentrations of further infrared active gases are plotted, since the most significant differences are visible there. Besides CO_2 and CO, CH_4, C_2H_4, C_2H_6 and EMC (See figures S4, S5, S6 and S8) show the same linear increasing trend. The very high concen-
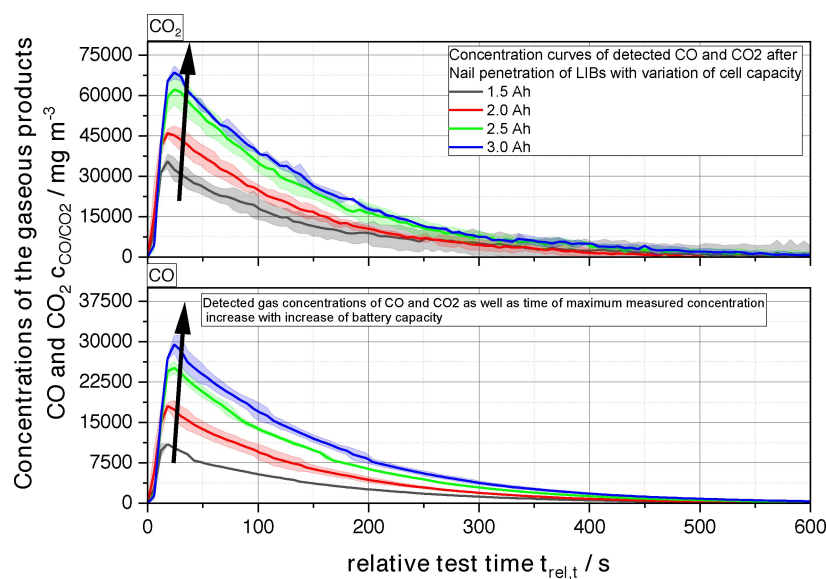

Figure 5. Concentration profiles over time of the infrared active gases CO_2 and CO at nail concentration of battery cells with 1.5 Ah (black), 2.0 Ah (red), 2.5 Ah (green), and 3.0 Ah (blue) capacity.

Batteries & Supercaps

Research Article
doi.org/10.1002/batt.202200060

Chemistry Europe
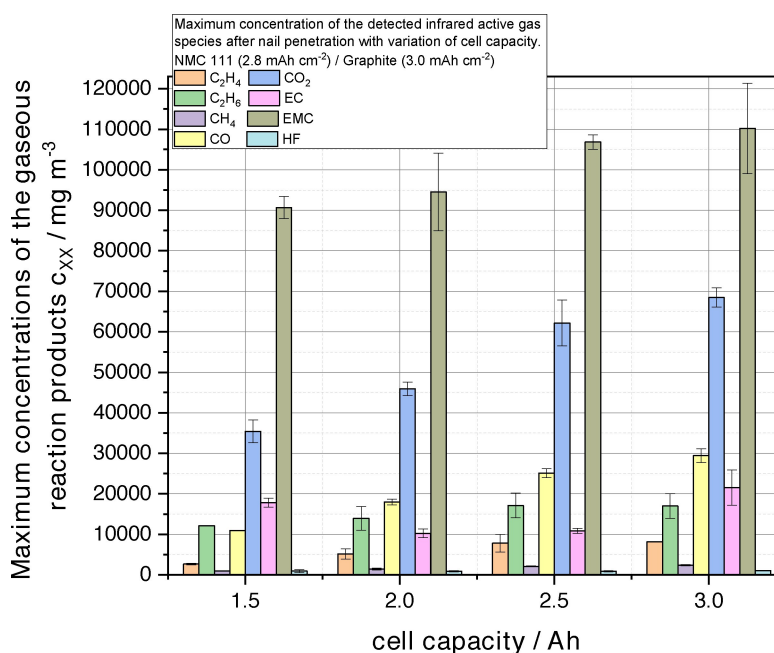European Chemical
Societies Publishing

Figure 6. Visualization of the maximum concentrations of measurable infrared active gas species released during TR in relation to the associated battery capacity.

trations of EMC are measured because it is the main component of the electrolyte. The increase in concentration from 90,658 mg cm^{-3} ± 2,730 mg cm^{-3} to 110,189 mg cm^{-3} ± 11,130 mg cm^{-3} is less than for CO and CO_2. Due to the higher temperatures at higher battery capacities, more EMC is decomposed and is measurable as a decomposition product, e.g., C_2H_6 or CO_2. CH_4, C_2H_4 and C_2H_6, like the other decomposition products, show an increase in concentration with increasing battery capacity. However, the determined slope of the concentration increase is lower than for CO_2 and CO because the intermediate decomposition products preferentially react further to the aforementioned CO and CO_2 at increasing temperatures and concentrations. The decomposition products are formed on a larger scale when larger amounts of reactant and higher temperatures are available at the same time. Despite the exothermic nature of the decomposition reactions, energy is required to exceed the activation energy to start the reactions. Therefore, the increase of the concentrations is mainly due to the larger amount of electrolyte or reactant and the higher temperature. Conversely, of course, the temperature also increases as more reactions take place. This explains the self-reinforcing effect of the TR very well. The measured concentrations of EC and HF show a deviating behavior in the maximum value (See Figures S7 and S9). EC shows minimum concentrations at 2.0 and 2.5 A h battery capacity and higher values at 1.5 and 3.0 A h. EC, as liquid electrolyte components, is also transferred to the gas phase during the reactions and participates in subsequent decomposition reactions. Nevertheless, the measured fraction should theoretically increase. It is likely that the EC crystallize on colder stainless-steel surfaces, such as those installed in the measurement setup as it is operated at room temperature

(approx. 20 °C), and is removed from the gas before the FTIR measurement. The measured concentrations of HF remain almost constant over the measuring range. The concentration of HF should also increase with increasing battery capacity due to the decomposition of the conductive salt $LiPF_6$ and the decomposition of the cathode binder PVDF. The constant measured concentration can also be explained on the one hand by condensation of HF on the cold stainless-steel surfaces and on the other hand by the high reactivity of HF, which makes detection difficult. For example, Essl et al. could not measure EC and HF at all in their experiments due to these processes.[14] EMC was also difficult to detect because it also condensed during cooling of the chamber and was removed from the gas phase.

In summary, with the use of FTIR gas measurements when varying the battery capacity with constant geometric dimensions of the electrodes, it was found that the maximum determined concentrations of the electrolyte component EMC increase in a linear relationship. Decomposition products also increase. Accordingly, EC shows a deviating behavior due to its crystallization point and is only partially accessible to gas measurement. The decomposition products of the two substances, CH_4, C_2H_4, C_2H_6, CO_2 and CO, show a linear increase in concentration, as EMC does. With the help of the determined dependencies, emerging concentrations of certain gaseous reaction products can be predicted. Thus, it is possible to parameterize simulations or to make estimates of the hazard potential with little testing effort.

Conclusion

The results of this work enable an approach to a model-like description of the processes involved in the TR of lithium-ion battery cells and the mapping of characteristic parameters that characterize the TR in more detail and describe its extent. The influence of battery cell capacity plays a particular role in the feasibility and interpretation of safety tests. Battery cells with a lower capacity have a lower hazard potential and can be tested with less effort, since the energy content, temperatures and released gas quantities are lower (battery cells with less than 1.5 A h capacity are not going into the TR). It could be shown in this work that characteristic points of the cell voltage, like the setoff point as well as the time until the cell voltage reaches 0 V after the start of the uncontrolled reaction, can be described with simple linear and nonlinear functions. Depending on the electrochemically stored energy released surface temperatures between 557.59 °C and 624.36 °C arise, whereby the increase over the increased capacities shows a linear characteristic. The maximum cell surface temperature decreases with increasing distance from the penetration point, but the gradient of the slopes decreases with increasing capacity between the measurement points. The temperature distribution over the surface becomes more uniform. As the temperature increases, the strength of the TR responses also increases. The required penetration depth decreases linearly and the mass loss due to the TR approaches a limit of 37.5%. The measured gas concentrations show a similar picture. With increasing capacity, the reactant quantities, in particular the electrolyte quantity, also increase and the released gas quantities of infrared-active gases increase. An almost linear increase as a function of capacity can be determined for all gases. Only EC and HF show a different trend, which, however, can be attributed to condensation behavior or crystallization behavior and high reactivity.

The transfer of the results and in particular the characteristic parameters to LIB of other geometric dimensions (e.g., enlargement of the electrode surface) or other cell formats (e.g., round cell, prismatic cell) is an essential point. When the electrode area is increased, the penetration depth of the nail to the TR is expected to decrease, since each compartment contains a larger amount of energy and resulting compensating currents from intact compartments as well as the expected Joule heat are larger at occurring smaller damages. Thus, TR may already occur with smaller defect cases. In this case, the temperatures reached on the cell surface depend on the capacity of the cells used but should also have higher values for higher capacities. If the format is varied, it can be expected that, depending on the cell design, the installed safety components will trip. Prismatic and round cells contain burst valves which are triggered when the internal cell pressure rises above critical values and discharge any gases produced. Pouch cells rupture indefinitely at the seal seams, as shown. Since electrode rolls in both formats are frequently used, it is to be expected, analogous to the stacks, that compensating currents will flow from intact areas into the damaged area and that a TR will be triggered. Depending on the width of the electrodes and the stored energy, the currents and the resulting Joule heat will also increase. Thus, with larger cells, even with these designs, it is to be expected that minor damage can already cause a TR. In today's, especially e-mobility, applications, battery cells with considerably larger capacities than those investigated in this test series are found for the most part. As discussed, according to our findings, the risk of a TR increases with higher capacity, even with smaller defects, if the cell is penetrated with a conductive object. Temperatures will reach higher values on the surface and the voltage drop, depending on electrode size, type of cell and capacity will change. If the area of the electrode is increased, it is expected that a smaller defect will be sufficient to trigger the TR due to larger amounts of stored energy. However, the time for the voltage to reach 0 V can be expected to increase when the number of electrode layers is increased and vice versa when the number of layers is decreased. If both the number of layers and the electrode area are increased, we expect the effects to overlap. A TR is already expected due to smaller defects, whereby the temperatures on the cell surface become higher with increasing capacity, but the time until the voltage reaches 0 V is determined with increasing or decreasing number of electrodes. Whether and to what extent the methodology has to be adapted, e.g., if both the capacity and the areal size of the electrodes are changed, will be investigated in subsequent research work."

In summary, the present results have shown that the TR and its responses as well as the effects can be described and represented by simple mathematical fits using an established, reproducible test methodology. These results can strongly contribute to design test safely and with great significance and also to establish down-scaling without loss of information.

Experimental Section

In the following, an approach to describe scale-dependent parameters in the thermal runaway of LIB is described. All experiments were performed in the battery cell investigation chamber with its integrated actuator and sensor technology and accompanying online FTIR gas analysis, as already described in previous work.[11,12] All results were determined by a triple determination in minimum.

Battery cell investigation chamber

Basically, the battery cell investigation chamber is a gas-tight chamber with an interior volume of 15.4 l constructed to perform mechanical battery abuse tests with the possibility of simultaneous measurement of infrared active gas species which is already described in previous work.[12] The chamber is designed to endure an internal pressure of 5 bar. This internal pressure can be generated during thermal runaway of LIB, since a large amount of gaseous reaction compounds is generated in short time (2–3 $L A^{-1} h^{-1}$ overall). To enable the gas measurement of infrared active gas species the chamber is connected to a Fourier-Transformation Infrared Spectroscope (FTIR, Gasmet Technologies GmbH, Karlsruhe, Germany) with an active dilution system. In operation mode, the chamber is constantly flowed through with nitrogen (5 ppm H_2O) for which the FTIR pumping unit and nitrogen gas feed is set to the constant volume flow of 6 $L min^{-1}$.

Batteries & Supercaps

Research Article
doi.org/10.1002/batt.202200060

Chemistry Europe
European Chemical
Societies Publishing

The resulting concentrations of the reaction gases in the gas mixture are further determined via the peak intensities using an algorithm from the manufacturer (Gasmet Technologies GmbH, Karlsruhe). The gases were measured in advance by the manufacturer of the system. During thermal runaway generated extra gas is exhausted to an extra piping system to protect the FTIR system. However, all generated gases are led into the gas scrubber before released into the environment. Furthermore, the chamber enables the measurement of internal pressure, internal temperature and allows video monitoring during the experiment.

Cell voltage is measured with crocodile clamps at the terminals. Cell surface temperatures are recorded by six thermocouples (type K, max. temperature 1200 °C) with a distance of 10, 20 and 30 mm from the penetration point as a double determination. Furthermore, the voltage-based nail control described previously[12] is used to stop the nail when thermal runaway starts. In this test series, a conductive steel nail with a tip angle of 30° and diameter of 3 mm is used.[11] A nail velocity of 1 mm s^{-1} based on the previous results[12] is chosen. The battery cells in this investigation are fixed under defined compression conditions of 0.166 MPa during the nail penetration experiments. The fixation is realized between two steel plates of 2 mm thickness. In addition, thermal insulation made of glass fiber tape (Coatis GmbH, Heidelberg, Germany) is inserted into the cell press on the top and bottom of the cell.

Investigated cells

The battery cells used in our study were manufactured in pouch cell format at the Battery LabFactory Braunschweig (Technische Universität Braunschweig, Germany). All cells were fabricated with NMC111 (2.8 mAh cm^{-2}) on the cathode side and graphite (3.0 mAh cm^{-2}) on the anode side. The electrodes are assembled by z-folding to multi-layer pouch cells. A trilayer PP/PE/PP polymer separator from Celgard (Celgard LLC, Charlotte, North Carolina, USA) with 20 μm thickness is used. The electrolyte mixture comprised of ethylene carbonate (EC) and ethyl methyl carbonate (EMC) in a gravimetric ratio of 3:7 wt.% with 2 wt.% venylene carbonate (VC) and 1 mol L^{-1} LiPF$_6$. All contacted packs were dried in a vacuum drying furnace for at least 16 h at 60 °C at a maximum pressure of 100 mbar, before they are filled with the calculated amount of electrolyte. Variations in capacity necessary for economies of scale were fabricated by changing the number of electrode layers, so cells were built with 1.0, 1.5, 2.0, 2.5, and 3.0 Ah capacities. For every multi-layer pouch cell, the capacity lies within a range of <1,5% of the specified value. The number of compartments (composite of anode – separator – cathode) was changed between 7, 10, 13, 16 and 19, while the outer dimensions of the electrodes were kept constant.

The cells were charged with 0.1 C (CCCV, cut off voltage 4.2 V) before the safety test were carried out. Further characteristic parameters of the cells are compiled in Table 4.

Furthermore, prior to the building cells with varying capacity, the electrolyte quantity of 3 cells each with a theoretical capacity of 1.0 Ah (7 compartments) was tested using an electrolyte amount of 20.5, 27.3, 34.1 and 41.0 mass.% versus the weight of the contacted cell stack. An internal resistance test by pulse test (1 s, 1 C charge/discharge) and a C-rate discharge test (charge 0.1 C CCCV/discharge 0.1 C, 0.2 C, 0.5 C, 1 C, 2 C) were performed after formation (2× charge 0.1 C CC/discharge 0.1 C CC, 1× charge 0.1 C CCCV/discharge 0.1 C CC) (Figures 7 and 8). It was found that cells with an electrolyte amount of 20.5 mass.% achieve a reduced discharge capacity after formation and at the same time have an increased internal resistance (charge 0.0246 ± 0.003 Ω, discharge 0.016 ± 0.002 Ω). In contrast, the investigated cells with 27.3, 34.1

Table 4. Technical data of the investigated battery cells. EMC: ethyl methyl carbonate, EC: ethylene carbonate, LiPF$_6$: lithium hexafluoro phosphate, LiNi$_{0.33}$Mn$_{0.33}$Co$_{0.33}$O$_2$: lithium nickel manganese cobalt oxide.

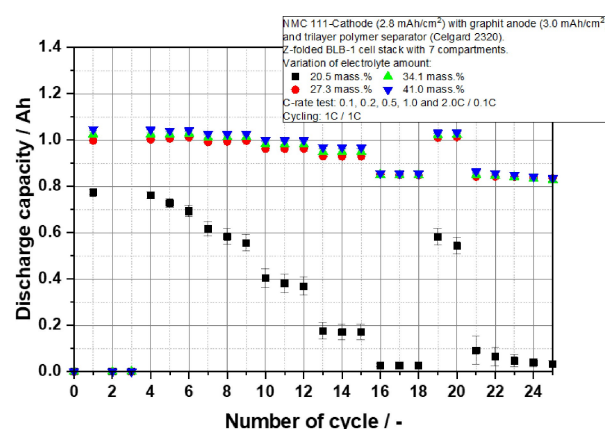| Parameter	Value
typ. capacity [Ah]	1.0, 1.5, 2.0, 2.5, 3.0
compartments (anode – cathode)	7, 10, 13, 16, 19
nominal voltage [V]	3.7
charge cut-off voltage [V]	4.2
discharge cut-off voltage [V]	2.9
electrolyte	EC/EMC (3:7 wt.%), 2 wt.% VC and 1 M LiPF$_6$
cathode active material	LiNi$_{0.33}$Mn$_{0.33}$Co$_{0.33}$O$_2$
cathode areal capacity [mAh cm^{-2}]	2.8
cathode area [mm × mm]	65 × 45
anode active material	Graphite
anode areal capacity [mAh cm^{-2}]	3.0
anode area [mm × mm]	70 × 50
total weight [g]	29, 39, 48.5, 58, 68
cell dimensions [mm × mm × mm]	107 × 102 × 5.9

Figure 7. Discharge capacity under variation of the electrolyte amount for 1 Ah pouch cells with NMC 111 and graphite electrodes
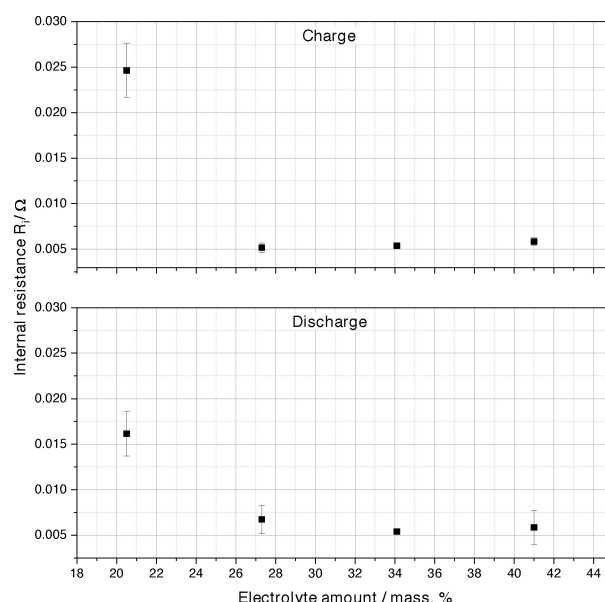

Figure 8. internal resistance values under variation of the electrolyte amount for 1 Ah pouch cells with NMC 111 and graphite electrodes.

Batteries & Supercaps

Research Article
doi.org/10.1002/batt.202200060

Chemistry Europe
European Chemical
Societies Publishing

and 41.0 mass.% of electrolyte show the expected discharge capacity of 1 Ah after formation and stable behavior in the C-Rate test. It can be seen that the cells filled with 27.3 mass.% show slightly worse behavior. When comparing the internal resistance during charging and discharging, the cells with 34.1 mass.% of electrolyte shows the lowest value. Therefore, it can be assumed that charge losses are lowest for this quantity. In this case, an insufficient amount of electrolyte leads to a lack of wetting of the electrode surfaces, which has a strong negative influence on the ionic conductivity. In the further course, all investigated cells of the capacity variation were built with an electrolyte quantity of 24.1 mass.% from the contacted cell stack.

X-Ray imaging

X-ray images of the cells before and after nail penetration test using the conductive nail are taken by Viscom AG (Hannover, Germany). The cells were irradiated from the penetration side with an X-ray inspection system (X8011-II PCB flex).

Acknowledgements

Conflict of Interest

The authors declare no conflict of interest.

Data Availability Statement

The data that support the findings of this study are available from the corresponding author upon reasonable request.

[1] C. Xu, Q. Dai, L. Gaines, M. Hu, A. Tukker, B. Steubing, *Commun. Mater.* **2020**, *1*, 437.
[2] A. Kwade, W. Haselrieder, R. Leithoff, A. Modlinger, F. Dietrich, K. Droeder, *Nat. Energy* **2018**, *3*, 290.
[3] R. Korthauer (Ed.) *Handbuch Lithium-Ionen-Batterien*, Springer Vieweg, Berlin u.a., **2013**.
[4] a) Y. Nishi, *Chem. Rec.* **2001**, *1*, 406; b) T. Placke, R. Kloepsch, S. Dühnen, M. Winter, *J. Solid State Electrochem.* **2017**, *21*, 1939.
[5] a) R. Spotnitz, J. Franklin, *J. Power Sources* **2003**, *113*, 81; b) Q. Wang, P. Ping, X. Zhao, G. Chu, J. Sun, C. Chen, *J. Power Sources* **2012**, *208*, 210.
[6] B. Mao, H. Chen, Z. Cui, T. Wu, Q. Wang, *Int. J. Heat Mass Transfer* **2018**, *122*, 1103.
[7] A. Nedjalkov, J. Meyer, M. Köhring, A. Doering, M. Angelmahr, S. Dahle, A. Sander, A. Fischer, W. Schade, *Batteries* **2016**, *2*, 5.
[8] J. L. Tebbe, T. F. Fuerst, C. B. Musgrave, *J. Power Sources* **2015**, *297*, 427.
[9] H. Yang, G. V. Zhuang, P. N. Ross, *J. Power Sources* **2006**, *161*, 573.
[10] a) J. Lamb, C. J. Orendorff, *J. Power Sources* **2014**, *247*, 189; b) V. Ruiz, A. Pfrang, A. Kriston, N. Omar, P. van den Bossche, L. Boon-Brett, *Renewable Sustainable Energy Rev.* **2018**, *81*, 1427.
[11] S. Doose, W. Haselrieder, A. Kwade, *Batteries* **2021**, *7*, 6.
[12] J. Diekmann, S. Doose, S. Weber, S. Münch, W. Haselrieder, A. Kwade, *J. Electrochem. Soc.* **2020**, *167*, 90504.
[13] M. Chen, Q. Ye, C. Shi, Q. Cheng, B. Qie, X. Liao, H. Zhai, Y. He, Y. Yang, *Batteries & Supercaps* **2019**, *2*, 874.
[14] C. Essl, A. W. Golubkov, A. Fuchs, *J. Electrochem. Soc.* **2020**, *167*, 130542.